The lattice parameters and widths of $PbTi_yZr_{1-y}O_3$ are given in Table 1 where a_r and α denote the transformed rhombohedral lattice parameters.

In addition to the basic series of samples, denoted as (I) (Table 1, Fig. 1), three more measurements were made for estimating the precision. Two are given in Table 1. For $y=0{\cdot}30$ the same sample was used as in the basic series, but the reference material was silver rather than aluminum. For $y=0{\cdot}38$ another sample of the same composition was used employing a different technique for polishing the sample surface. A third measurement was made to compare the reference materials. Here silver was used as the reference material and the lattice parameter of aluminum was determined as for the pseudocubic samples. The measured value of aluminum was $4{\cdot}0496_4$ Å at 25 °C in agreement with the reported value of 4·0496 Å.

On the basis of these results, it is concluded that the precision of the determination of the lattice parameters of $PbTi_yZr_{1-y}O_3$ in this study is of the order of 0·005%.

References

CERNOHORSKY, M. (1961). *Czech. J. Phys.* B**11**, 684.

CERNOHORSKY, M. (1968), *Rozpravy C.S.A.V.* (Czechoslovak Academy of Sciences), **78**, No. 5.

HNILICKA, M. & KARMAZIN, L. (1969). *Czech. J. Phys.* A**19**, 276.

PEARSON, W. B. (1967). *A Handbook of Lattice Spacings and Structures of Metals and Alloys*, Vol. 2. London: Pergamon Press.

Acta Cryst. (1972). A**28**, 187

Electron Microscope Study of an Homologous Series of Shear Structures based on Molybdenum Trioxide

BY L. A. BURSILL

School of Chemistry, University of Western Australia, Nedlands, W.A. 6009, *Australia*

(*Received* 8 *June* 1971)

Electron microscopy and diffraction evidence is presented for the existence of four new molybdenum oxides Mo_nO_{3n-2}, $n=19$, 20, 21, and 22.

Introduction

The structural chemistry of the higher molybdenum oxides MoO_x, $2{\cdot}00 \le x \le 3{\cdot}00$, was thoroughly studied by Magnéli and Kihlborg. They determined and/or refined the crystal structures of MoO_2, Mo_4O_{11}(monoclinic), Mo_4O_{11}(orthorhombic), $Mo_{17}O_{47}$, Mo_5O_{14}, Mo_8O_{23}, Mo_9O_{26} (monoclinic), $Mo_{18}O_{52}$(triclinic), and MoO_3 (see review by Kihlborg, 1963*a*). Magnéli (1953) introduced the idea of homologous series to describe the structural relationship between Mo_8O_{23}, Mo_9O_{26} and an hypothetical MoO_3 with ReO_3-type structure. He proposed a method for deducing the unit cell and atomic positions for unknown members of the series. Further members were then found in the mixed oxides $(Mo,W)_nO_{3n-1}$ with $n=10$, 11, 12, and 14. There was almost complete agreement between the observed and predicted structures.

It has remained puzzling that Magnéli phases with $n \ge 10$ did not appear in the pure molybdenum oxides. Instead Mo_9O_{26} and MoO_3 appeared to be the only stable phases between 750 °C and the melting point 790 °C. A completely different structure, $Mo_{18}O_{52}$, coexisted with MoO_3 at lower temperatures. Single-crystal studies showed it to be derived from MoO_3 rather than ReO_3 (Kihlborg, 1963*b*). Kihlborg proposed that this was the first member of a new homologous series $Mo_nO_{3n-m+1}(MoO_3)$ with $n=18$, $m=3$, and $x=2{\cdot}8889$. His X-ray patterns suggested that at least four other phases existed but were rare, could not be prepared reproducibly, and were presumed metastable. Approximate unit-cell parameters were derived for two of these and a comparison with the ideal values suggested that they may be $Mo_{13}O_{38}$($n=13$, $m=2$, $x=2{\cdot}9231$) and $Mo_{26}O_{75}$($n=26$, $m=4$, $x=2{\cdot}8864$).

Later X-ray studies have revealed a large number of ReO_3 based homologous series (the block structures) in the niobium oxides and oxyfluorides MX_x, $2{\cdot}4 \le x \lesssim 2{\cdot}7$ (Wadsley & Andersson, 1970). The term crystallographic shear (CS) structures was introduced to describe the formal relation between the members of such series and the parent structures (Wadsley, 1955).

Electron optical studies of TiO_x (Bursill, Hyde, Terasaki & Watanabe, 1969; Bursill & Hyde, 1971) and of $(Ti,Cr)O_x$ (Bursill, Hyde & Philp, 1971) in the composition range $1{\cdot}89 \le x \lesssim 1{\cdot}98$ have revealed numerous homologous series Ti_nO_{2n-a} ($1 \le a \lesssim 30$) derived from rutile by CS. The X-ray studies (Andersson & Jahnberg, 1963) suggested that the one known series $4 \le n \le 9$ merely extended to higher n values. On the contrary new structural principles emerged giving a continuous series of ordered phases reminiscent of the proliferation of phases around Nb_2O_5. These new phases could not be detected by X-ray diffraction due to their special reciprocal lattice geometry.

We therefore chose to study MoO_x, $2{\cdot}89 \le x \lesssim 3{\cdot}00$,

in the belief that similar principles as occurred in the ReO_3 and TiO_2 based oxides would also occur here.

Specimen preparation and examination

Several samples with $2{\cdot}89 \leq x \leq 3{\cdot}00$ were prepared by thoroughly mixing appropriate weights of molybdenum and molybdenum trioxide powders (Koch–Light 3*N*). About 5g of each mixture was sealed in a quartz tube (previously ignited in air at 800 °C), heated for various times in horizontal resistance furnaces, and finally quenched to room temperature in water. Four temperatures from 600 to 800 °C were used. The following results refer to only one sample, starting composition $MoO_{2{\cdot}90}$, which was sealed at 10^{-4} torr of air and heated at 810 °C for 10 hours then at 748 °C for 72 hours. Well developed crystalline products were fractured between glass microscope slides, mounted on specimen grids and examined in a JEM-6A or ELMISKOP 101 electron microscope. The accelerating potential was 100 kV, anticontamination devices were used and thin flakes were carefully oriented using a goniometer stage.

Observations

Many flakes gave diffraction patterns as shown in Fig. 1. The strong spots are indexed using MoO_3 indices (suscript *M*). Short rows of 'superlattice' spots, apparently along the reciprocal lattice vector $\mathbf{g}(30\bar{1})_M$, accompany each strong MoO_3 spot. Note that there is no such row through the origin. The superlattice rows are therefore inclined to this $(010)_M$ reciprocal lattice plane. We therefore tilted about an axis normal to the superlattice rows until a zone was found with complete rows through all the MoO_3 spots, including the origin (Figs. 2, 3, and 4). Twenty such patterns were obtained from different crystals. In each case the superlattice rows were parallel to $\mathbf{g}(35\bar{1})_M$. Often several superlattice spacings were obtained from one flake. The spots varied from very sharp to broad and streaked. Fig. 5 shows a lattice image obtained from a crystal giving a streaked pattern. One fringe spacing predominates but lamellae of one or two wider spacings occur at irregular intervals.

Five periodicities were measured on the sharp patterns, *i.e.* 19·5, 20·7, 21·8, 23·0, and 24·0 Å (±1%), corresponding to 17, 18, 19, 20, and 21 spots along $\mathbf{g}(35\bar{1})_M$. Occasionally MoO_3 patterns with no superlattice occurred and some patterns proved Mo_4O_{11} was also present.

Structural principles and derivation of ideal unit cells

Molybdenum trioxide is usually regarded as zigzag strips of edge-shared MoO_6 octahedra along $[001]_M$ joined by corner sharing to form sheets parallel to $(010)_M$ at two levels (Fig. 6). Each octahedron has one unshared corner giving the appearance of a layer structure. The free apices in one layer point down between those of neighbouring layers. Ideally the oxygen packing is f.c.c. with Mo in one third of the octahedral interstices. Fig. 7(*a*) shows the pattern of filled interstices for an *A* layer. This is repeated on *B* and *C*, being merely offset as required for f.c.c. and to generate the zigzag edge-shared arrangement in Fig. 6.

An idealized layer of $Mo_{18}O_{52}$ is shown projected onto $(010)_M$ in Fig. 8(*a*). The parent MoO_3 is divided into slabs infinite in two directions but with 2×18 octahedra along the zigzag rows. Each slab is displaced by $[\frac{1}{2}\mathbf{a}_M - \frac{1}{6}\mathbf{b}_M]$* relative to the next. Kihlborg's *b* and *c* axes [Fig. 8(*a*)] may be written

$$\mathbf{b} = 1\mathbf{a}_M + 3\mathbf{c}_M$$
$$\mathbf{c} = \tfrac{9}{2}\mathbf{a}_M + \tfrac{1}{6}\mathbf{b}_M - 3\mathbf{c}_M \, .$$

* Actually $[\frac{1}{2}\mathbf{a}_M - \frac{1}{7}\mathbf{b}_M]$ in the real structure.

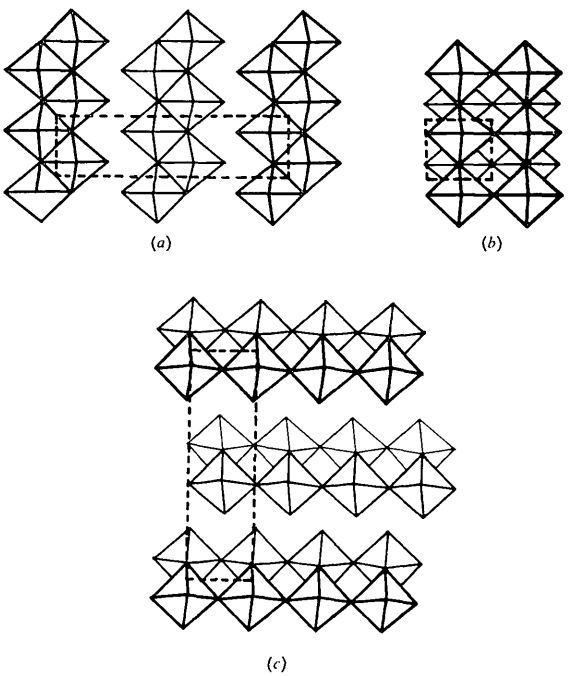

Fig. 6. (*a*) $[100]_M$, (*b*) $[010]_M$, (*c*) $[001]_M$ projections of MoO_3

Table 1. *Comparison of observed and ideal cell parameters for* $Mo_{18}O_{52}$, $Mo_{13}O_{38}$, *and* $Mo_{26}O_{75}$

		a	*b*	*c*	α	β	γ
$Mo_{18}O_{52}$	obs	8·145 Å	11·89 Å	21·23 Å	102·67°	67·82°	109·97°
	calc	8·097	11·771	21·09	102·17	68·50	110·32
$Mo_{13}O_{38}$	obs	8·6	8·46	21·5	97	67	116
	calc	7·852	8·387	21·12	93·65	69·9	114·5
$Mo_{26}O_{75}$	obs	10·41	15·43	23·72	98·27	84·47	137·71
	calc	10·32	15·307	23·13	93·7	83·4	137·9

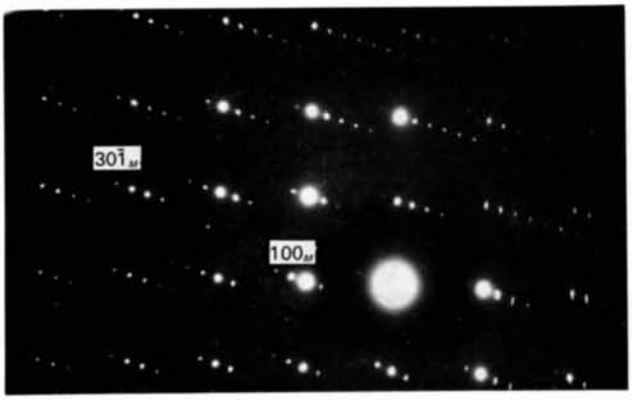

Fig. 1. $[010]_M$ zone of typical flake of $MoO_{2\cdot90}$. Superlattice rows appear parallel to $\mathbf{g}(30\bar{1})_M$ but there is no row through the origin.

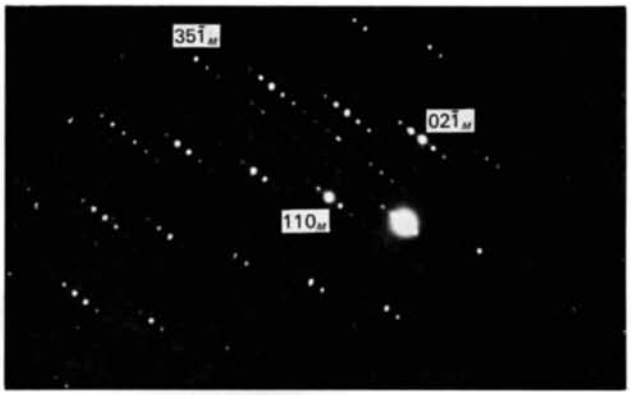

Fig. 2. $[\bar{1}12]_M$ zones of $MoO_{2\cdot90}$ showing 17, 18, 19, 20, and 21 spots along $\mathbf{g}(351)_M$.

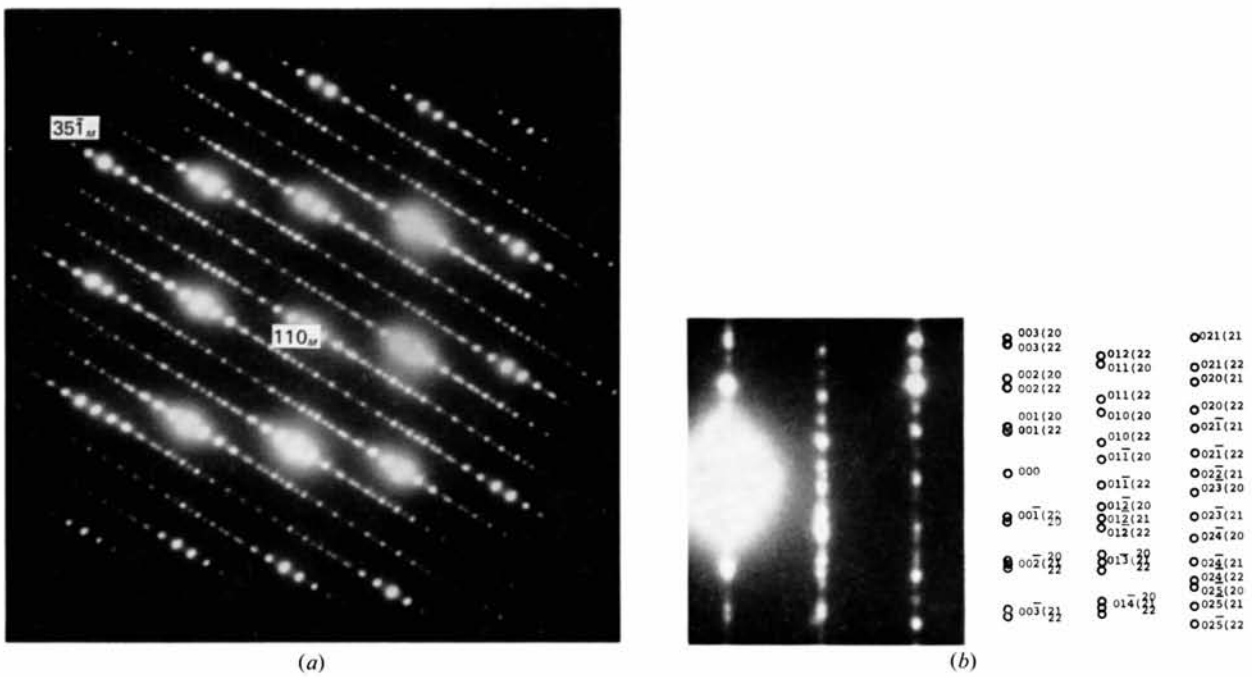

Fig. 3. (*a*) $[\bar{1}12]_M$ zones of $MoO_{2\cdot90}$ showing 17, 18, 19, 20 and 21 spots along $\mathbf{g}(351)_M$. (*b*) Indexed central area of (*a*): brackets refer to *n*.

[*To face p.* 188

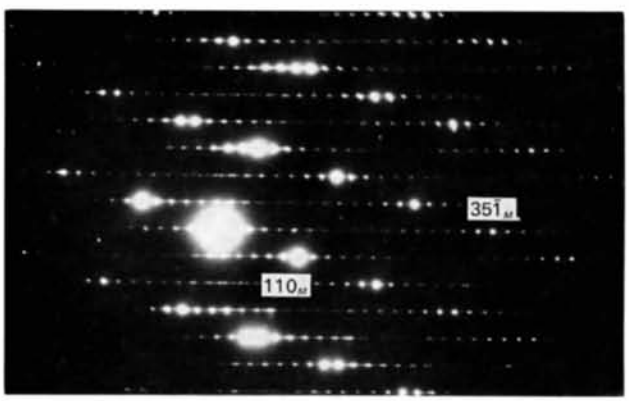

Fig. 4. $[\bar{1}12]_M$ zones of $MoO_{2\cdot90}$ showing 17, 18, 19, 20 and 21 spots along $g(351)_M$.

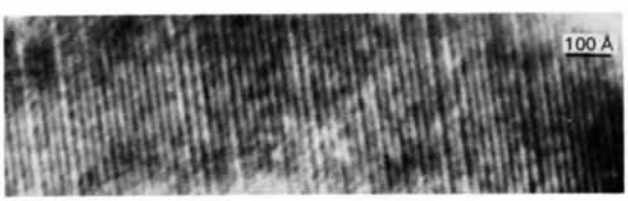

Fig. 5. Lattice fringe image obtained from a crystal giving a streaked diffraction pattern (main spacing is $n=20$).

In $Mo_{18}O_{52}$ one Mo atom at the ends of each zigzag row has tetrahedral coordination, reducing the amount of edge-sharing (Kihlborg, 1963*b*), but not affecting the stoichiometry or the ideal unit cell.

The oxygen sites formally eliminated from MoO_3 and the resulting pattern of filled interstices in $Mo_{18}O_{52}$ are indicated in Fig. 7 (*a*) and (*b*) Note that the anion lattice is recovered after the shear operation. Of the four close-packed planes it was convenient to project onto $(13\bar{1})_M$ in Fig. 7 because both the CS vector and Kihlborg's **a** axis lie in this plane. We see that

$$\begin{aligned}\mathbf{a} &= -2[\tfrac{1}{2}\mathbf{a}_M+\tfrac{1}{2}\mathbf{c}_M]+3[\tfrac{1}{2}\mathbf{a}_M-\tfrac{1}{6}\mathbf{b}_M]\\ &= \tfrac{1}{2}\mathbf{a}_M-\tfrac{1}{2}\mathbf{b}_M-1\mathbf{c}_M\,.\end{aligned}$$

Note that **a** and **b** define the infinite extent of the basic structure, *i.e.* the CS *plane*, whereas **c** defines the width of basic structure, *i.e.* the CS plane *spacing*. The CS plane (hkl) contains the vectors $\mathbf{a}=[u_1v_1w_1]$ and $\mathbf{b}=[u_2v_2w_2]$, *i.e.*

$$\begin{aligned}h&=v_1w_2-v_2w_1=-\tfrac{3}{2}\\ k&=w_1u_2-w_2u_1=-\tfrac{5}{2}\\ l&=u_1v_2-u_2v_1=\tfrac{1}{2}\text{ , }i.e.\ (35\bar{1})_M\,.\end{aligned}$$

We write the CS operation as $[\frac{1}{2}\mathbf{a}_M-\frac{1}{6}\mathbf{b}_M]\,(35\bar{1})_M$.

The *a* and *b* axes are independent of *n* but **c** (see Fig. 8(*b*) and (*c*) for ideal layers of $Mo_{19}O_{55}$ and $Mo_{20}O_{58}$) becomes

$$\mathbf{c}=\tfrac{9}{2}\mathbf{a}_M+\tfrac{1}{6}\mathbf{b}_M-(n-15)\mathbf{c}_M\,.$$

The unit cell parameters for Mo_nO_{3n-2} are therefore related to those of MoO_3 by the matrix

$$\begin{array}{ccc}\frac{1}{2} & -\frac{1}{2} & -1\\ 1 & 0 & 3\\ \frac{9}{2} & \frac{1}{6} & 15-n\,.\end{array}$$

The ideal values deduced for $Mo_{18}O_{52}$ are in excellent agreement with those observed (Table 1).

The *b* and *c* axes for Mo_nO_{3n-1} and Mo_nO_{3n-3} homologues may be derived as above (Fig. 8(*d*) and (*e*) shows $Mo_{13}O_{38}$ and $Mo_{26}O_{75}$). Kihlborg did not deduce ideal *a* axes for these. We did so by a trial and error method which resulted in the following matrices

$$\begin{array}{lccc}Mo_nO_{3n-1} & 0 & \frac{1}{2} & -1\\ & 1 & 0 & 2\\ & \frac{9}{2} & \frac{1}{6} & 10-n\\ Mo_nO_{3n-3} & -\frac{1}{2} & \frac{1}{2} & -2\\ & 1 & 0 & 4\\ & \frac{11}{2} & \frac{1}{6} & 24-n\end{array}$$

All six ideal cell parameters for $Mo_{26}O_{75}$ and five of the six for $Mo_{13}O_{38}$ are in good agreement with the observations (Table 1). The difference for **a** in the latter may reflect the relative inaccuracy of the data used as no other MoO_3 vectors could be found to give

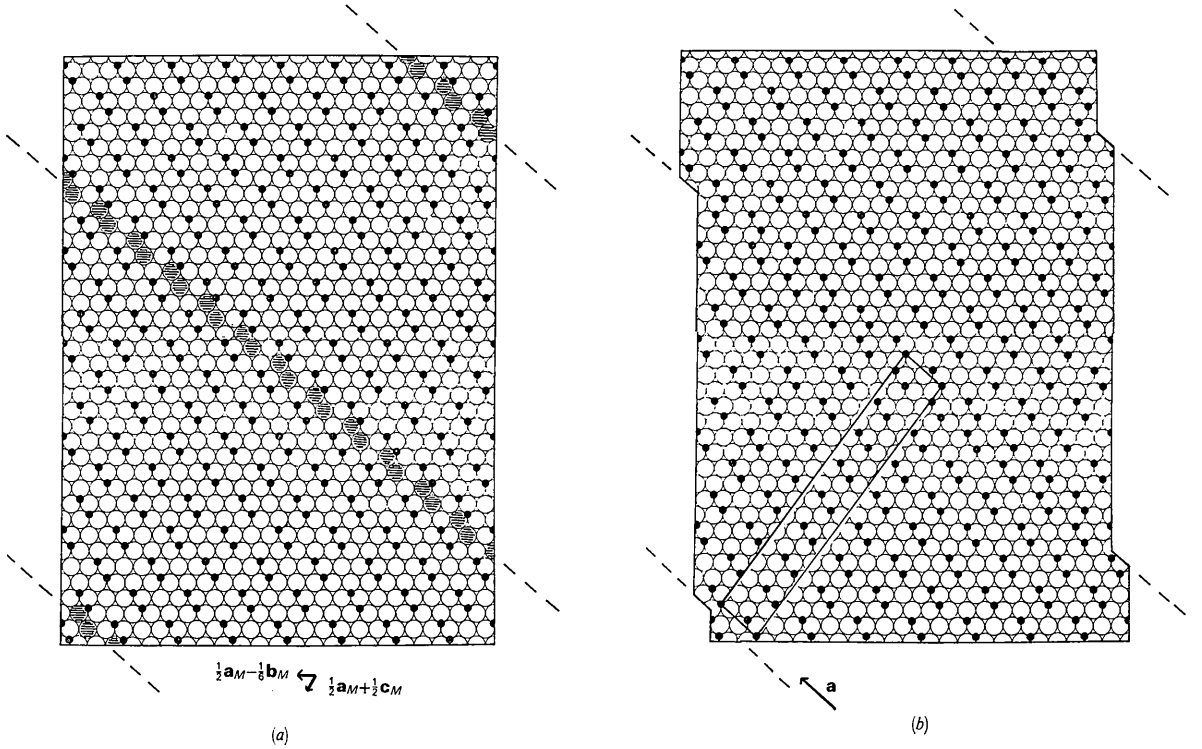

Fig. 7. Pattern of filled octahedral interstices in the ideal f.c.c. anion lattices of (*a*) MoO_3 and (*b*) $Mo_{18}O_{52}$. Larger shaded circles in (*a*) indicate anion sites eliminated formally by the CS operation $[\frac{1}{2}\mathbf{a}_m-\frac{1}{6}\mathbf{b}_M](35\bar{1})_M$.

better agreement for all six parameters. The a and b axes above define the CS planes to be $(\bar{2}21)_M$ for Mo_nO_{3n-1} and $(40\bar{1})_M$ for Mo_nO_{3n-3}.

Indexing the diffraction patterns

The observed superlattice rows were always along $\mathbf{g}(35\bar{1})_M$. We therefore used the first matrix. Table 2 lists the ideal unit cell parameters for Mo_nO_{3n-2}, $17 \le n \le 25$. From the matrix we see that $35\bar{1}_M$ transforms to 00, $n-\frac{2}{3}$, *i.e.* there are $n-\frac{2}{3}$ superlattice spots along $\mathbf{g}(35\bar{1})_M$. The CS plane spacing is given by $D_{sp} = d_{35\bar{1}M}(n-\frac{2}{3})$. An approximate n may be obtained by indexing the MoO_3 subcell positions and calculating a camera constant. n may be assigned unambiguously only by a detailed comparison of observed and calculated d values and interplanar angles. Table 3 lists some of these for low order reflexions in $[\bar{1}12]_M$, *i.e.* [100] for Mo_nO_{3n-2}. The angle between 001 and $01\bar{1}$ provides a sensitive measure of n. For example an indexed enlargement of the centre of Fig. 3(*a*) is shown in Fig. 3(*b*). The measurements were made directly on a

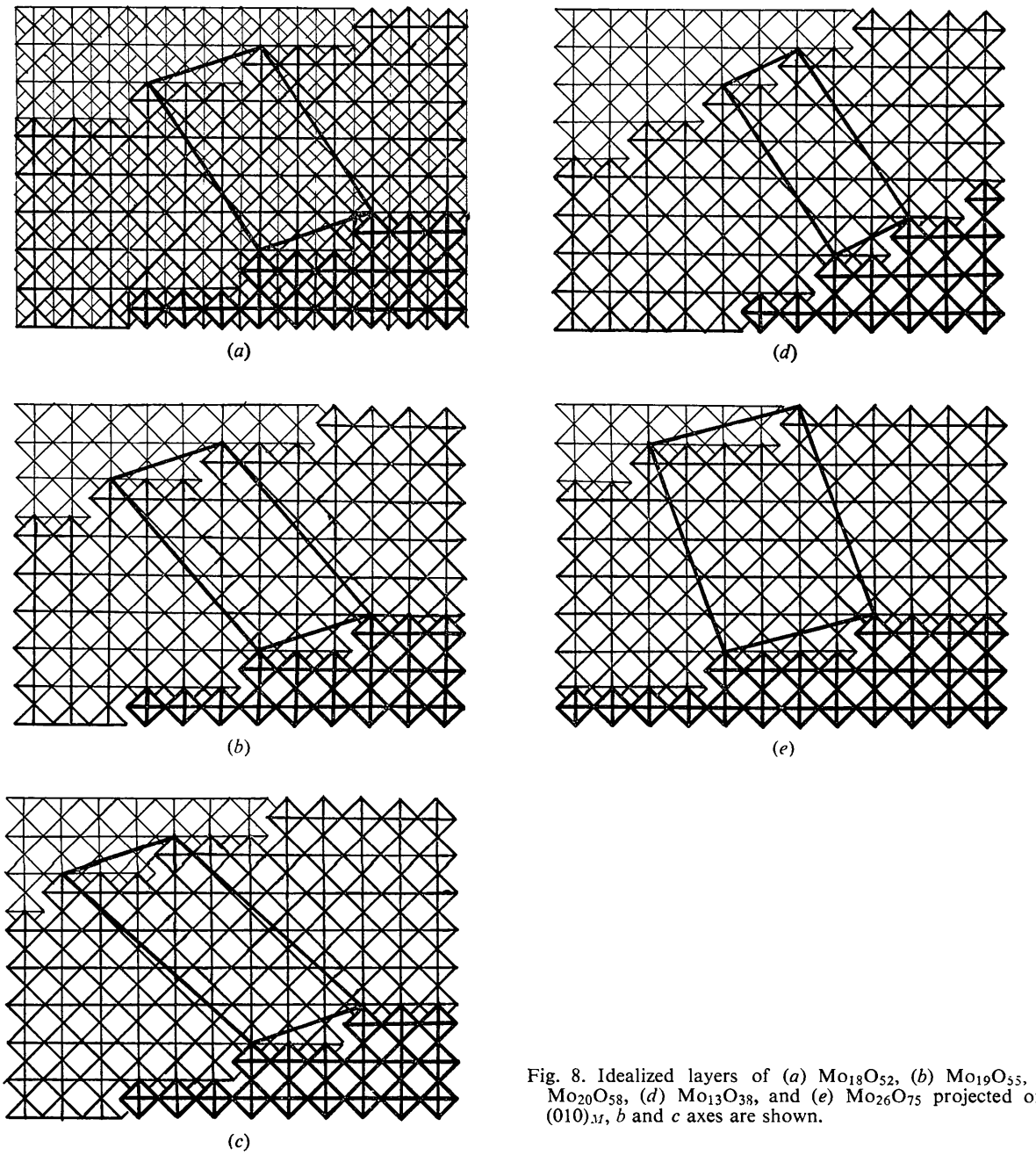

Fig. 8. Idealized layers of (*a*) $Mo_{18}O_{52}$, (*b*) $Mo_{19}O_{55}$, (*c*) $Mo_{20}O_{58}$, (*d*) $Mo_{13}O_{38}$, and (*e*) $Mo_{26}O_{75}$ projected onto $(010)_M$, b and c axes are shown.

photographic enlarger. All the observed patterns could be indexed in a straightforward manner, within experimental error, including those from different zones. Altogether five n values were obtained; 18, 19, 20, 21 and 22.

Table 2. *Ideal cell parameters for* Mo_nO_{3n-2}, $17 \leq n \leq 25$

$a = 8{\cdot}097$, $b = 11{\cdot}771$ Å, $\gamma = 110{\cdot}32°$ for all phases.

n	x	c	α	β
17	2·8823	19·406 Å	92·83°	71·85°
18*	2·8889	21·092	102·17	68·50
19*	2·8947	23·249	109·93	66·17
20*	2·9000	25·759	116·28	64·45
21*	2·9048	28·527	121·47	63·35
22*	2·9091	31·487	125·68	62·62
23	2·9130	34·589	129·18	62·13
24	2·9166	37·798	132·10	61·80
25	2·9200	41·088	134·53	61·60

* Observed in this study.

Table 3. *D values and angles for some low-order reflexions*

n	d	hkl	Angle between 001 and hkl
18	10·10 Å	$01\bar{1}$	64·65°
	11·12	010	95·62
	19·53	001	–
19	10·71	$01\bar{1}$	73·41
	10·86	010	103·65
	20·67	001	–
20	11·07	$01\bar{1}$	81·95
	10·47	010	110·39
	21·78	001	–
21	11·18	$01\bar{1}$	90·05
	10·04	010	116·05
	22·90	001	–
22	11·08	$01\bar{1}$	97·35
	10·59	$01\bar{2}$	71·44
	9·61	010	120·71
	24·04	001	–

Discussion

Only $Mo_{18}O_{52}$ was positively identified in the X-ray studies. Apparently this lowest member of the series was obtained as a reasonably pure product by suitable heat treatment and careful selection of crystals. The higher members always occur as mixtures. As the total composition range is only 0·027 in the metal/oxygen ratio and D_{sp} varies from 19·5 to 24·0 Å they could conceivably be dismissed as disordered metastable non-equilibrium phases. The lattice image (Fig. 5) suggests that diffuseness or streaking on the diffraction patterns is due to thin lamellae of a second n. For wider lamellae the diffraction spots become sharper (unmixing). If there were no tendency to unmix, ordered intergrowth of adjacent n values might occur. The former appears to hold here.

Kihlborg observed one member of each series $m = 2$, 3 and 4 and concluded that certain n values of each series have increased stability due to the distortions which exist in the real structures. (The CS plane rotates rather than changes spacing as the stoichiometry is varied.) Following our work on CS structures in rutile-based systems, where rotation did occur, we were surprised to find, contrary to Kihlborg's results, that n and not m was the variable. Our results do not exclude other CS planes in this system. We attempted to make other CS structures by varying the starting composition and the reaction temperature but failed. We did observe $(120)_M$ CS planes in very slightly reduced MoO_3 but these were disordered and often ended inside the crystal at a partial dislocation (Bursill, 1969). Further attempts to study the transition from $(120)_M$ to $(35\bar{1})_M$ CS planes are being made using ternary systems.

Thanks are due to Dr B. G. Hyde of the Chemistry Department and to Dr L. N. D. Lucas of the Electron Microscopy Centre of this University for providing facilities, and to the Australian Research Grants Committee and the U. S. Air Force Office of Scientific Research Grant No. AFOSR-69-1806 for financial support.

References

ANDERSON, S. & JAHNBERG, L. (1963). *Ark. Kemi*, **21**, 413.
BURSILL, L. A. (1969). *Proc. Roy. Soc.* A**311**, 269.
BURSILL, L. A., HYDE, B. G., TERASAKI, O. & WATANABE, D. (1969). *Phil. Mag.* **20**, 347.
BURSILL, L. A. & HYDE, B. G. (1971). *Acta Cryst.* B**27**, 210.
BURSILL, L. A., HYDE, B. G. & PHILP, D. (1971). *Phil. Mag.* **23**, 1501.
KIHLBORG, L. (1963*a*). *Ark. Kemi*, **21**, 471.
KIHLBORG, L. (1963*b*). *Ark. Kemi*, **21**, 443.
MAGNÉLI, A. (1953). *Acta Cryst.* **6**, 495.
WADSLEY, A. D. (1955). *Rev. Pure Appl. Chem.* **5**, 165.
WADSLEY, A. D. & ANDERSSON, S. (1970). *Perspectives in Structural Chemistry*, Vol. 3, p. 1. Edited by J. D. DUNITZ & J. A. IBERS. New York: John Wiley.